Supporting Information

Charge Carrier Transport Properties of Twin Domains in Halide Perovskites

Dohyung Kim[¶,3,10], Jae Sung Yun[¶,*,1,2], Arun Sagotra[3], Alessandro Mattoni[4], Pankaj Sharma[3,9,11], Jincheol Kim[6], Da Seul Lee[1], Sean Lim[7], Padraic O'Reilly[8], Liz Brinkman[8], Martin A. Green[1], Shujuan Huang[6], Anita Ho-Baillie[1], Claudio Cazorla[4], and Jan Seidel[3,9]*

[1] Australian Centre for Advanced Photovoltaics (ACAP), School of Photovoltaic and Renewable and Engineering, University of New South Wales, Sydney 2052, Australia

[2]Department of Electrical and Electronic Engineering, Advanced Technology Institute (ATI), University of Surrey, Guildford GU2 7XH, UK

[3] School of Materials Science and Engineering, University of New South Wales, Sydney 2052, Australia

[4]Department de Física, Universitat Politècnica de Catalunya, Campus Nord B4-B5, Barcelona, E-08034 Spain

[5] Consiglio Nazionale delle Ricerche, Istituto Officina dei Materiali, CNR-IOM, Cittadella Universitaria, Monserrato 09042-I, Cagliary, Italy

[6] School of Engineering, Macquarie University, Sydney, New South Wales, 2109 Australia

[7] Electron Microscopy Unit, University of New South Wales, Sydney 2052, Australia

[8] Molecular Vista, San Jose, CA 95119, USA

[9] ARC Centre of Excellence in Future Low-Energy Electronics Technologies (FLEET), UNSW Sydney, Sydney 2052, Australia

[10] Photovoltaics Research Department, Korea Institute of Energy Research, Daejeon 34129, Republic of Korea

[11] College of Science and Engineering, Flinders University, Adelaide, South Australia, Australia

†Correspondence: j.yun@unsw.edu.au, jan.seidel@unsw.edu.au
¶These authors contributed equally.

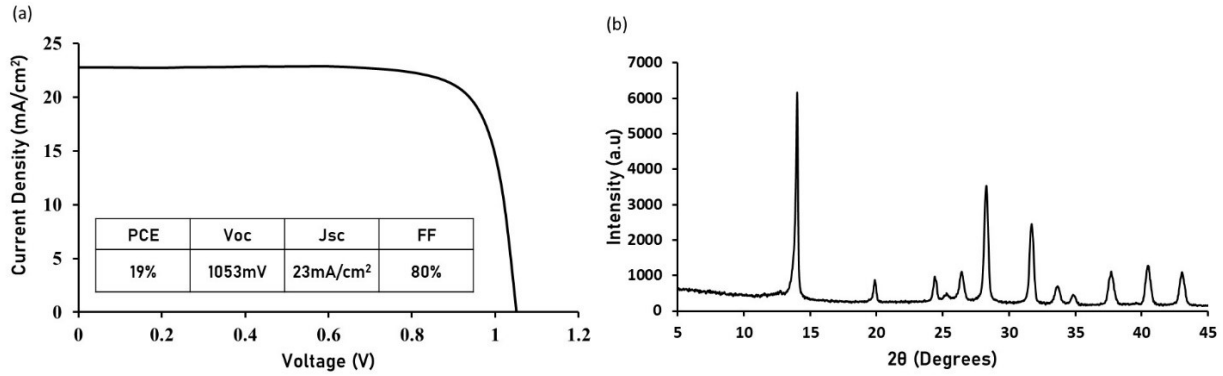

Fig. S1. (a) Reverse direction (V_{oc} to J_{sc}) *J-V* curve of perovskite solar cell consisting of FTO/c-TiO_2/m-TiO_2/ $(FAPbI_3)_{0.85}(MAPbBr_3)_{0.15}$/Spiro-MeOTAD/gold. (b) XRD patterns of a TiO_2/ $(FAPbI_3)_{0.85}(MAPbBr_3)_{0.15}$ layer. The characteristic perovskite peaks of (110), (200), (202), (220), and (222) are indexed to 14.0, 19.9, 24.44, 28.3, and ~31.82°, respectively.

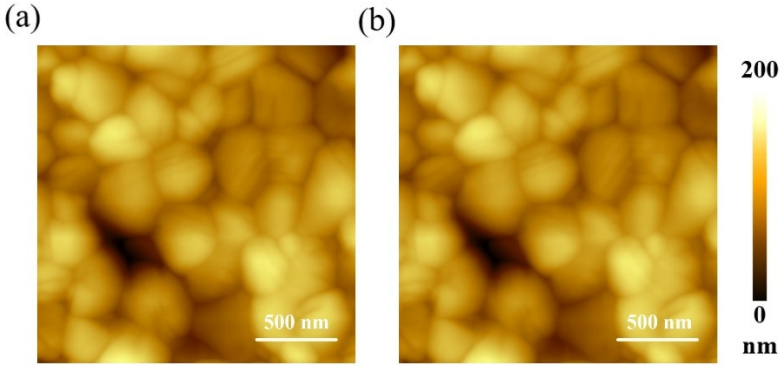

Fig. S2. Topography images including multigrain structures (a) before and (b) after a series of AFM measurements at the same region.

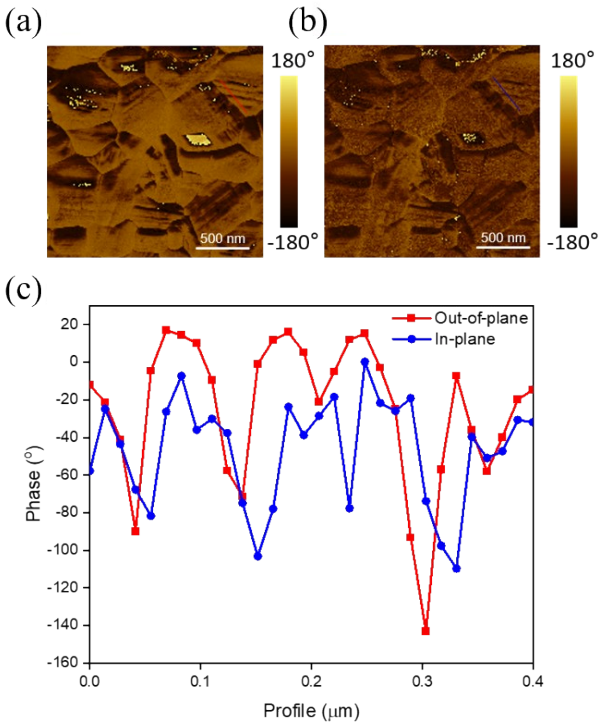

Fig. S3. (a) Out-of-plane and (b) in-plane PFM phase maps. (c) The corresponding line profiles of the red and blue lines in (a) and (b). The a-c domains can exist with out-of-plane and in-plane PFM signals simultaneously. Here, out-of-plane phase signals corresponding to up- or down-polarized responses are detected and in-plane signals next to out-of-plane signals are observed as perpendicular polarization directions of out-of-plane polarization directions.

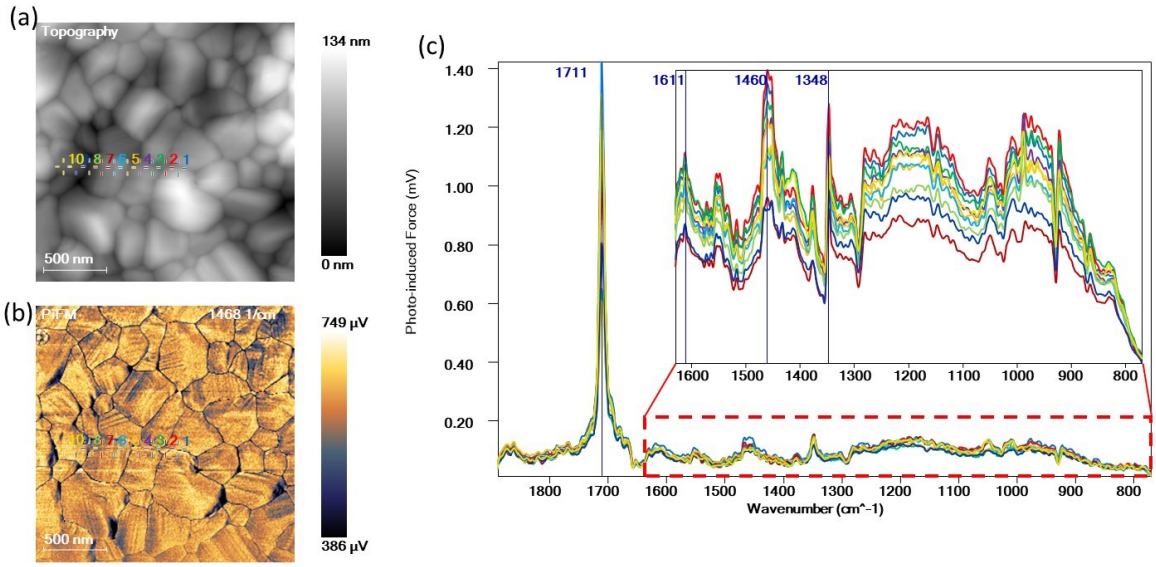

Fig. S4. (a) Topography (b) PiFM maps of $(FAPbI_3)_{0.85}(MAPbBr_3)_{0.15}$ perovskites. (c) PiFM spectra for the wavenumber range from 770 to 1890 cm^{-1} with intensity range of 0.1-0.5 mW.

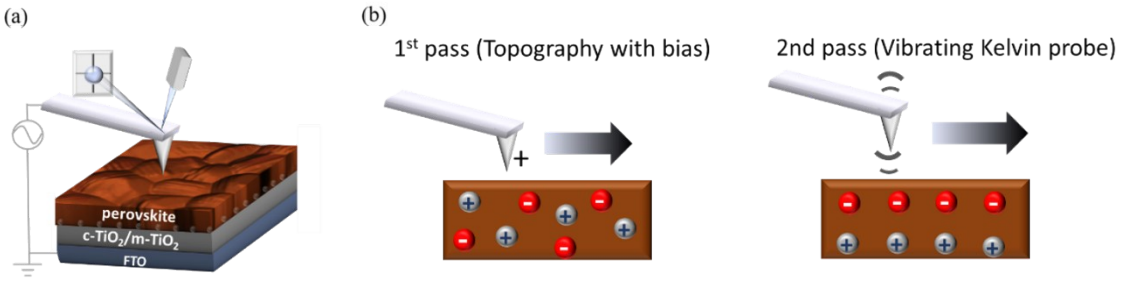

Fig. S5. Illustration of the (a) KPFM setup used in this work and (b) two-pass KPFM mode (non-contact) with mobile ions residing in the sample surface.[1]

Supplementary Note 1: KPFM

During the first pass, a bias is applied to the tip (positive in this example), attracting negative ions to the top surface of the film and repels positive ions to the bottom of the film. In the second pass, CPD is measured using a Kelvin probe mode. 200 pixels by 200 pixels are chosen with a scan rate of 1Hz. 200 pixels were scanned horizontally first then this topography is retraced and contact potential difference (CPD) is measured in the second pass. The delay time between the first and the second pass can be varied by scanning speed or scanning pixel density. Usually, a delay time of 900 ms is used. Consecutive KPFM measurements at different regions are carefully performed to exclude ion-related effects. Once the bias-dependent KPFM measurements are carried out, excited ions are not fully relaxed within several hours. Thus, the series of KPFM measurements under both positive and negative biases are performed in different regions. Our KPFM was operated in the amplitude modulated mode, so-called AM-KPFM. Typically, the AM-KPFM suffers from a strong electrostatic force as compared to frequency-modulated KPFM (FM-KPFM), while better potential sensitivity can be obtained using AM-KPFM.[2] Particularly, as the perovskites are sensitive materials, to minimize the electrostatic effect, we carefully optimize the experimental conditions such as the distance between the AFM tip and film surface, applied tip bias, life height, the delay time between first and second passes, In many cases, if the conditions are not optimized, appropriate scanning images cannot be obtained due to an electrostatic background.

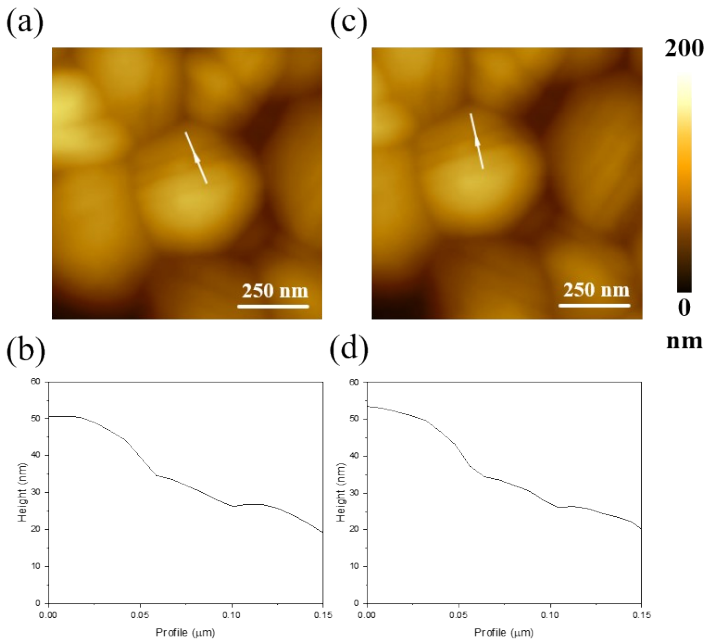

Fig. S6. Evidence of unchanged topography (a-b) before and (c-d) after the measurement over 2 hours at ~25℃ with a relative humidity of 30-40%.

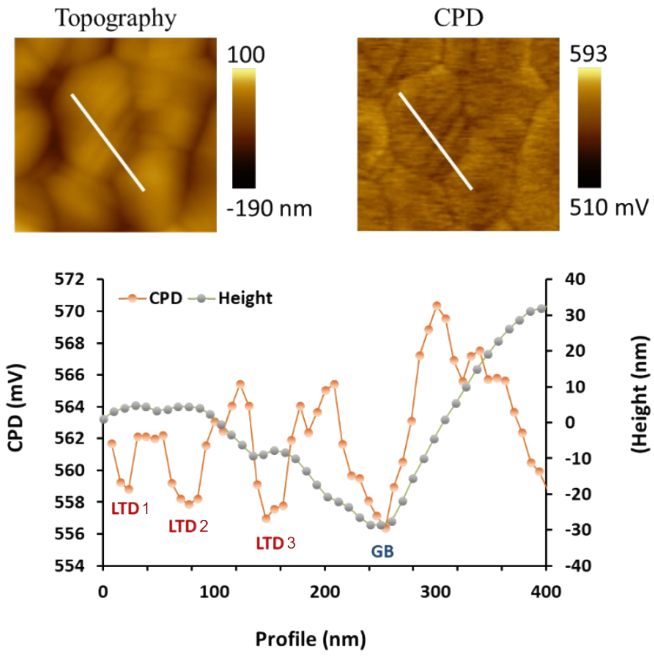

Fig. S7. Topography and CPD maps and profiles of white lines showing domain patterns and grain boundaries. We confirm that CPD profiles do not exactly follow the height profile, for example, CPD of LTD3 (558 mV) is comparable to the grain boundary (556 mV) despite LTD3 is located 20 nm higher in height. This indicates that the CPD values are not dependent on the height difference, rather, determined by their exclusive electrical properties.

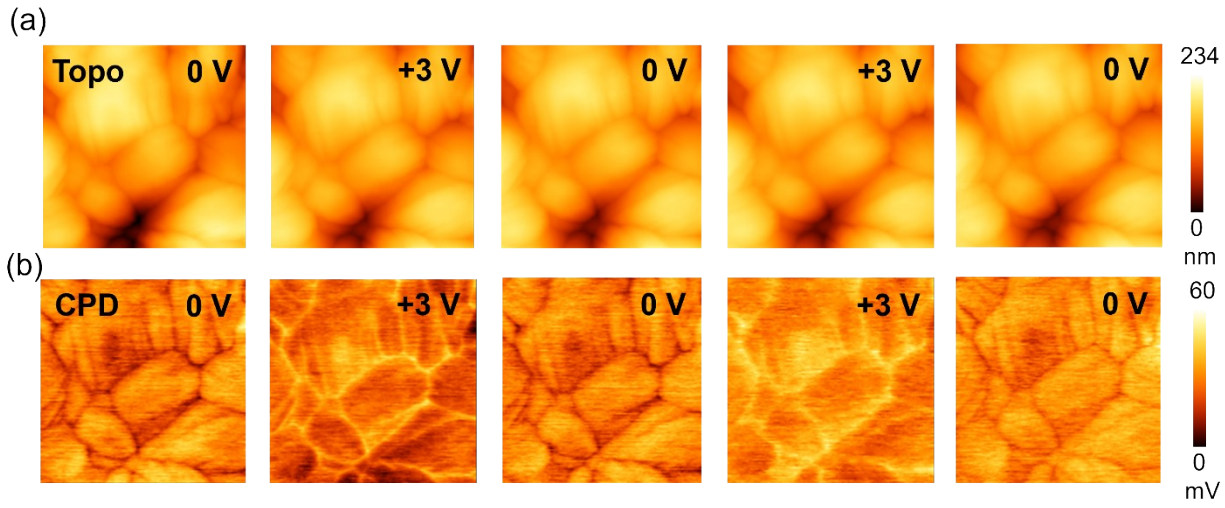

Fig S8. The series of a) topography and b) the corresponding CPD images when + 3V bias voltage is on and off.

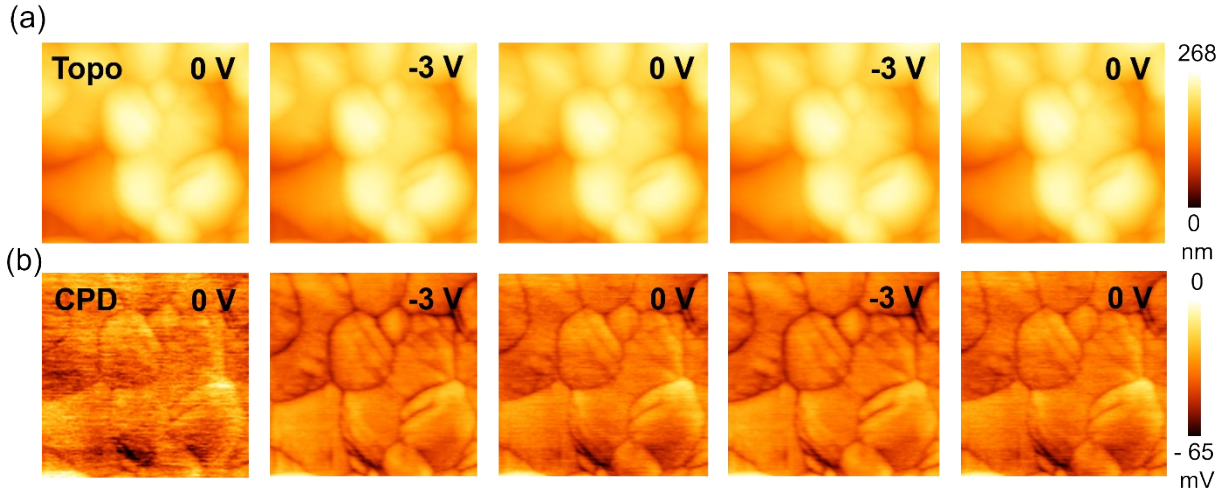

Fig S9. The series of a) topography and b) the corresponding CPD images when - 3V bias voltage is on and off.

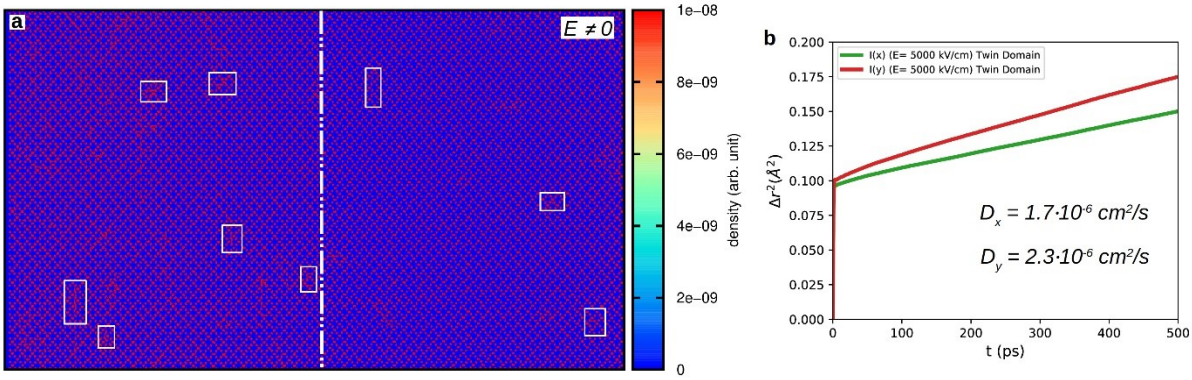

Fig. S10. Iodide ionic diffusivity properties calculated in the 90º ferroelastic twin domain system at T = 300 K and E = 5,000 kV/cm. **a.** Iodine density plot calculated for the configurations generated during a 1,000 ps molecular dynamics run; red areas indicate high occupancy probability of I ions whereas blue areas low occupancy probability. Few local ionic diffusion processes are indicated with white boxes and the boundary between the two ferroelastic domains is highlighted with a white dashed-dotted line. Ionic diffusion occurs more or less homogeneously within the twin-domain system. **b.** Mean-squared displacement of I ions calculated in the direction of the applied electric field and domain wall, y = [010], and perpendicular to it, x = [100]. The diffusion of the iodine atoms is significantly larger along the y direction.

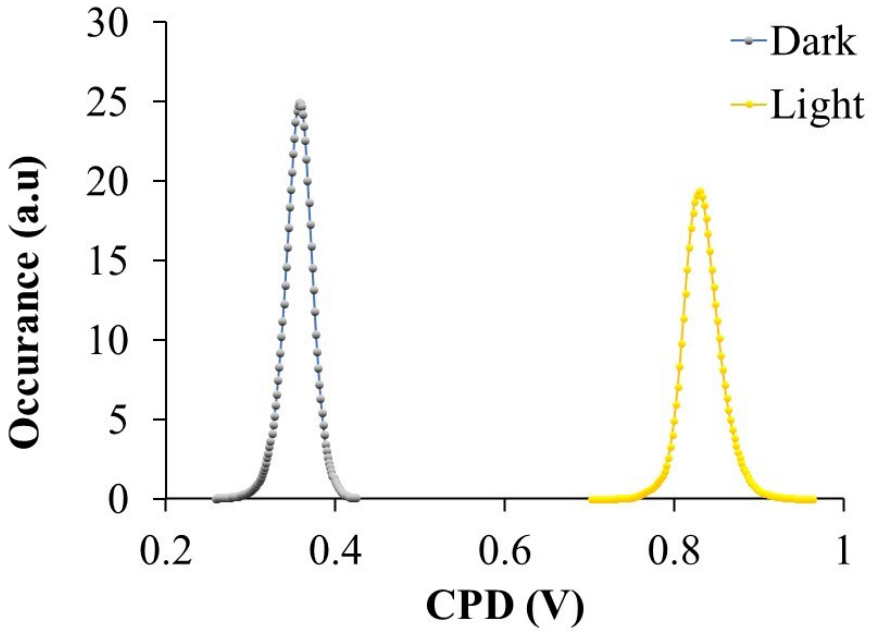

Fig. S11. CPD pixel distribution in dark (Figure 3(b)) and light (Figure 3(c)).

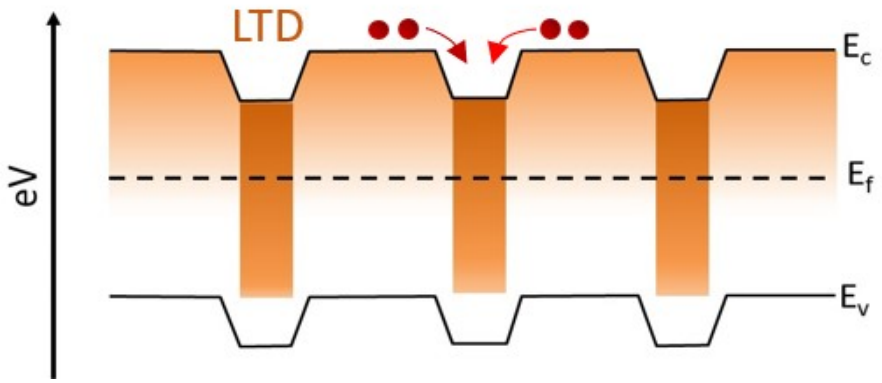

Fig. S12. Schematic illustration of band structure of LTDs and HTDs.

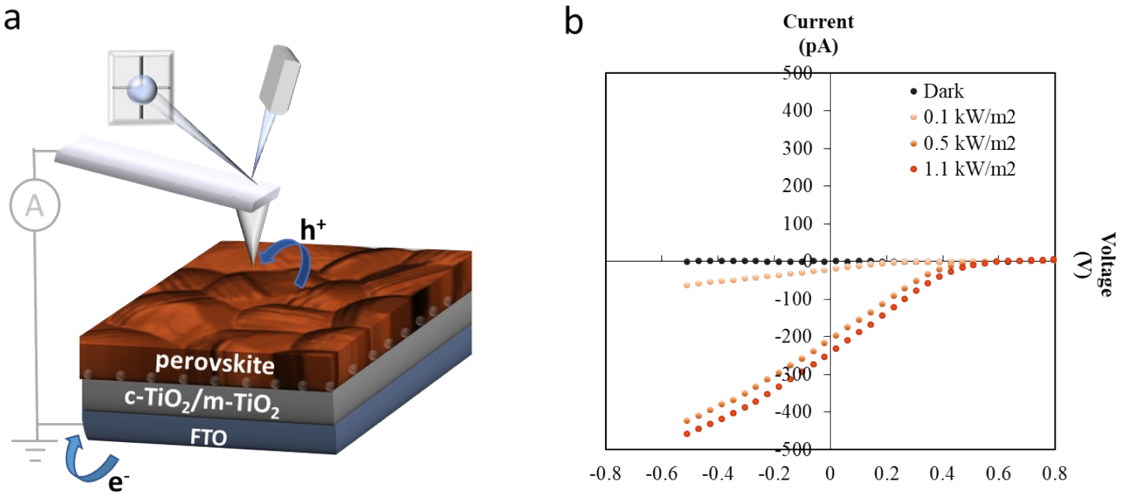

Fig. S13. (a) Conductive-AFM (c-AFM) setup used in this work. An electric circuit is established between the top sruface of the perovskite by a gold tip and FTO. (b) Resulting in light intensity I-V curves obtained from our c-AFM configuration which exhibit PV diode characteristics.

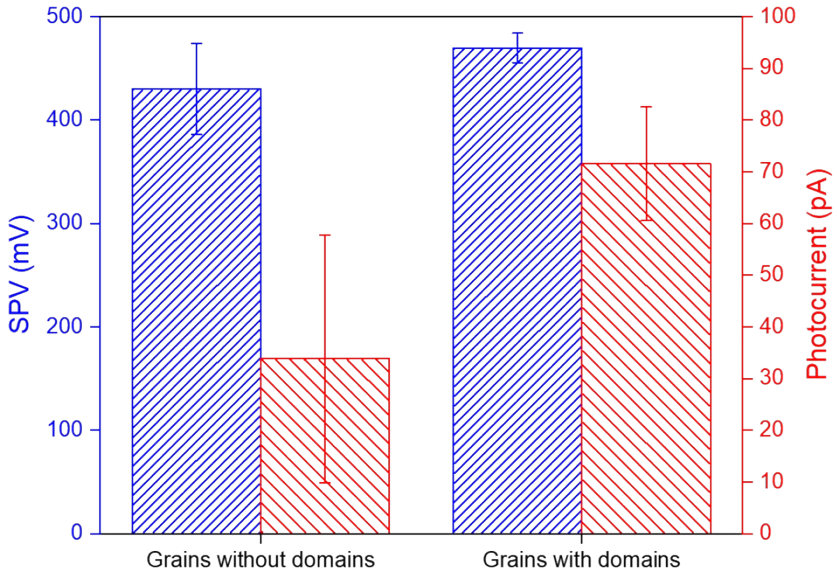

Fig. S14. The statistic surface photovoltage and photocurrent at grains with domains and grains without domains. These results were obtained from 10 grains with and without domains, respectively.

References

1. J. S. Yun, J. Seidel, J. Kim, A. M. Soufiani, S. Huang, J. Lau, N. J. Jeon, S. I. Seok, M. A. Green and A. Ho-Baillie, *Adv. Energy Mater.*, 2016, **6**, 1600330.
2. L. Collins, M. B. Okatan, Q. Li, I. I. Kravenchenko, N. V. Lavrik, S. V. Kalinin, B. J. Rodriguez and S. Jesse, *Nanotechnol.*, 2015, **26**, 175707.